CRYSTAL GROWTH & DESIGN

Article

Cite This: Cryst. Growth Des. XXXX, XXX, XXX−XXX

pubs.acs.org/crystal

Nanoparticle Assembly Leads to Mackinawite Formation

Adriana Matamoros-Veloza,*[,†,‡] Tomasz M. Stawski,[‡,§] and Liane G. Benning*[,‡,§,∥]

[†]School of Mechanical Engineering, University of Leeds, Leeds LS2 9JT, U.K.

[‡]School of Earth and Environment, University of Leeds, Leeds LS2 9JT, U.K.

[§]German Research Centre for Geosciences, GFZ, 14473 Potsdam, Germany

[∥]Department of Earth Sciences, Free University of Berlin, 12249 Berlin, Germany

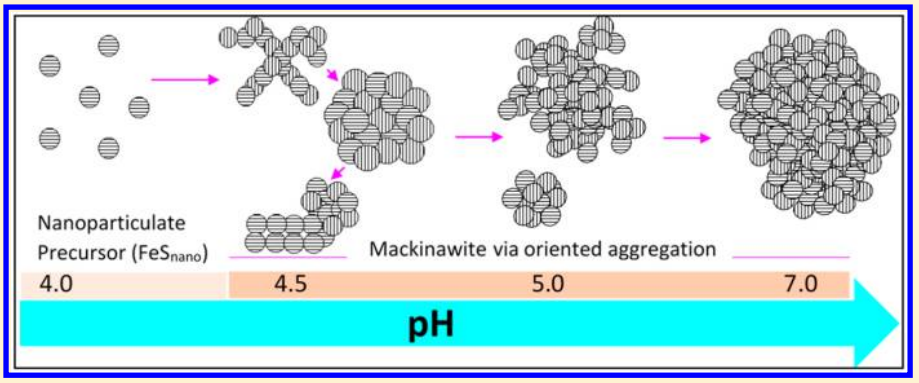

ABSTRACT: Iron sufides are important mineral phases in natural environments where they control global elemental cycles. Fe−S phases have been suggested to form through the transformation of several possible precursors to finally reach stable crystalline structures. Mackinawite is a metastable intermediate, of which a full chemical and structural characteristization of various possible intermediate stages in its formation pathways, or the chemical conditions that affect the transformations to the metastable mackinawite, are well understood. Here we report, the various steps of mackinawite formation via oriented aggregation (OA) from a nanoparticulate precursor. During OA, the formation of aggregates is a crucial stage for self-assembly of primary particles to reach stable structures. The formation occurs in five steps: (1) homogeneous nucleation of primary FeS_{nano} particles; (2 and 3) formation of mass fractal-like aggregates from the FeS_{nano} as precursor toward the transformation to mackinawite; (4) oriented alignment and self-assembly of these mackinawite-like aggregates; and (5) transformation to a still metastable but typical layered mackinawite structure.

INTRODUCTION

Iron sulfide phases (Fe−S) control several biogeochemical processes in modern and ancient environments.[1] Pyrite (FeS_2) is the dominant, crystalline, and stable iron sulfide mineral on Earth, and pyrite forms through the transformation of various mostly nanoparticulate, poorly ordered, and metastable Fe−S phases.[1−3]

Among iron sulfides, mackinawite is known to be a precursor to the more stable greigite[4,5] and pyrite.[1,4] In a recent study, we reported the existence of a solid, metastable iron sulfide nanophase that is a prerequisite precursor to poorly ordered mackinawite.[6] However, the knowledge about the nature and structure of intermediates in the mackinawite formation pathway is still incomplete. We do not understand what the chemical factors controlling the rates at which such precursors form, transform, and/or crystallize to mackinawite are.

This is despite the fact that nanophase precursors in the Fe−S system[6] are mirroring crystallization reactions in many other common mineral systems (e.g., iron oxides, carbonates, calcium sulfate, etc.)[7−9] where nucleation, growth, and transformation to more stable phases also proceeds through multiple aqueous and solid transitions.[8−19]

To fill this gap, we present here data from a study where we investigated the pathways and mechanisms of the initial stages of mackinawite formation through a nanophase Fe−S precursor that we previously documented as a prerequisite in any iron sulfide phase formation reaction.[6] By performing diffusion and titration experiments with sulfide from pH < 4 to pH 7 and under strict O_2-free conditions, we followed the formation of mackinawite from acidic ferrous solution. We elucidate how the reactions proceed through various intermediate stages until they reach mackinawite and derived mechanistic insights of solid transformations and changes in the structure during mackinawite growth. We propose a new mechanism for the formation of poorly crystalline mackinawite, which involves various assembly modes of primary precursor nanoparticles.

Received: July 6, 2018
Revised: September 18, 2018
Published: September 25, 2018

DOI: 10.1021/acs.cgd.8b01025
Cryst. Growth Des. XXXX, XXX, XXX−XXX

EXPERIMENTAL SECTION

Diffusion and titration experiments were performed following previously described methods.[6] A precipitation reaction was initiated by mixing an Fe^{2+} containing solution and sulfide, with the latter being either $H_2S_{(g)}$ (diffusion experiments, 1 and 24 h) or NaHS solutions (titration experiments 520 min). All solution preparations used deionized O_2-free water prepared freshly for each experiment.

Diffusion experiments were performed in a glovebox by diffusing $H_2S_{(g)}$ over a 0.1 M Fe^{2+} solution. Both reactants were prepared fresh before the experiments: $H_2S_{(g)}$ was produced by reacting ∼1 g of $Na_2S{\cdot}9H_2O$ (Sigma-Aldrich 99.999%) with 6 M HCl, and the Fe^{2+} solution was prepared from Mohr's salt, i.e. $(NH_4)_2Fe(SO_4)_2{\cdot}6H_2O$ (ACS Sigma-Aldrich 99%). Each diffusion experiment was replicated three times.

Titration experiments were performed by adding NaHS solutions to an Fe^{2+} containing solution in an Infors chemostat reactor with a continuous N_2 (99.99%) flow. Ferrous iron solutions were prepared from Mohr's salt as in the diffusion experiment, but the NaHS solutions were prepared from $Na_2S{\cdot}9H_2O$ [$Na_2S{\cdot}9H_2O$; Sigma-Aldrich 99.999%] following reported methods.[4,6,20] Titrations of 0.1 M Fe^{2+} solutions (pH 4.1) and 0.15, 0.5, and 1 M NaHS solutions to reach a pH of 7 were performed using a NaHS addition rate of 0.47 mL/min. Experiments performed using 0.5 and 0.1 M of NaHS for the titration revealed that the reaction was ∼15−50 times faster with a pH increase from 4.1 to 6.5−7.0 within the first minutes of reaction. Therefore, we performed all the experiments of this work using 0.15 M NaHS to capture at least the three stages of growth. The pH, Eh, volume of NaHS solution, and time were recorded automatically every minute, and each titration experiment was replicated 3 times. Full details of the experimental setup and synthesis methods are described by Matamoros et al. (2018).[6]

In situ and time-resolved small-angle X-ray scattering (SAXS) measurements were used to follow reactions in the titration of 0.1 M Fe^{2+} solution with 0.15 M NaHS solution at beamline I22 at the Diamond Light Source (UK). The solution/suspension from the chemostat reactor was circulated in a closed loop containing a custom-built PEEK cell with a borosilicate round capillary (ID = 0.998 mm) using a peristaltic pump. This setup allowed SAXS patterns to be collected from the samples passing through the capillary that was aligned with the X-ray beam. The station was set up to use a monochromatic X-ray beam at 12.4 keV and a Dectris Pilatus 2M detector located at 3.2 m from the capillary to collect two-dimensional scattering information in a q-range between 0.3 and 7.0 nm^{-1}. Transmission was measured using a photodiode in a beam-stop of the SAXS detector. The q-range for analysis was calibrated using silver behenate. Before each experiment, we collected a background signal from an empty capillary and from a capillary filled with water. The absolute intensity scale was calibrated with a 1 mm glassy carbon sample.[21] Scattering patterns were collected at 1 s/frame from the beginning of the reaction up to 30 min and then up to 9 h at a frame rate of 20 s/frame. SAXS data were background-subtracted, normalized, and integrated to 1D using the DAWN software package (v. 1.4).[22]

For solid characterization, intermediates and end products were removed from both the diffusion and titration experiments anaerobically using airtight syringes connected to a three-way valve with a N_2 flush inlet. After removal, the solids were filtered using 0.02 μm polycarbonate membranes and redispersed in O_2-free ethanol inside a glovebox. Solids were analyzed using X-ray diffraction (XRD) and transmission electron microscopy (TEM). For XRD analysis, redispersed samples were mounted onto a flat silicon surface in an airtight XRD holder inside the anaerobic chamber, dried, and scanned from 2° to 70° 2θ at 0.05°/min using a Bruker D8 diffractometer. XRD data were compared against the diffraction data of the crystal structure of mackinawite (AMCSD 0014518).[23] For TEM analysis, diluted samples were deposited onto holey carbon grids on copper TEM grids (Agar Scientific) and mounted into an anaerobic holder (Gatan 648 Double tilt). The samples were transported from the glovebox to the instruments in double-jacketed containers and three layers of plastic bags sealed inside a glovebox. Acquisition of HR TEM images was performed using a transmission electron microscope (FEI Tecnai TF20) fitted with a CCD Camera (Gatan Orius SC600A) and an energy dispersive X-ray (EDX) spectrometer (Oxford Instruments 80 mm^2 X-max). The microscope was operated at 200 kV. All the images were analyzed using the ImageJ software. Lattice spacings were obtained from fast Fourier transform of the images.

RESULTS AND DISCUSSION

The rate of nucleation, growth, and crystallization of solid phases were controlled by the volume of NaHS (titrations) or H_2S gas (diffusion) added over time. In all titrations the fastest change in pH from an initial pH of 4.1 to 5.2 was reached in the first 5 min (region I, Figure 1). During this stage a black

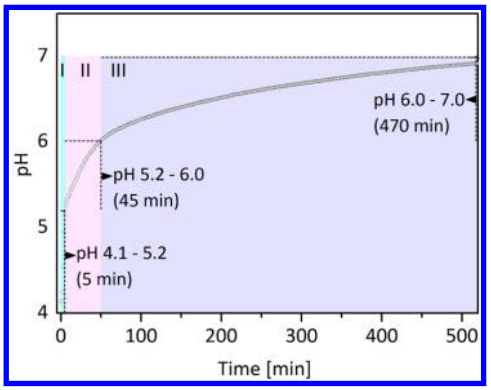

Figure 1. Stages in the evolution of the pH as a function of time for the titration of Fe^{2+} with 0.15 M NaHS.

precipitate formed via a further slower increase in pH from 5.2 to 6.0 within 45 min (region II, Figure 1), and a very slow rate of increase from pH 6.0 to ∼7.0 lasting 470 min (region III, Figure 1) produced a final jet black slurry.

Time-resolved SAXS patterns from the titrations of aqueous Fe^{2+} and 0.15 M NaHS over the full course of reaction also showed distinct intensity profiles with multiple stages (Figure 2a first 50 min; Figure 2b final 470 min). Overall, the intensity increased ∼1400-fold over the entire q-range and along the full time of the reaction between pH 4.1 and 7.0. Over the first 50 min of titration between pH 4.1 and 6.0, we observed an overall ∼23-fold increase in intensity at low q ($q < 1$ nm^{-1}) and the linear dependence of intensity in the log−log representation was attributed to the formation of mass-fractal-like aggregates. The general relatively constant intensity at high-q in the first hour and up to pH 6.0 was also an indication of the formation of large Fe−S aggregate structures composed of primary particles (Figure 2a). The increasing intensity in the low-q part of the data lacked a clear plateau (i.e., $I(q) \propto q^0$ scaling) suggesting that the sizes of the aggregates were infinitely large and that in our measurements the size information fell out of the q-range (Figure 2a). Over the next 470 min of reaction, the scattering intensity increased ∼60-fold along the entire q-range when the system further evolved from pH 6.0 to 7.0 (Figure 2b). Within this pH range, the distinctive features of the form factor, observed early in the process, were not visible anymore as the linear region extended to high-q values in the log−log plot. When the reaction reached pH 7.0, a local maximum appeared at $q_{max} = 3.3$ nm^{-1} corresponding to the characteristic average interparticle correlation distance of $2\pi/q_{max} = \sim 2$ nm (Figure 2b and 2c). This feature likely originated from either or both, the particles

DOI: 10.1021/acs.cgd.8b01025
Cryst. Growth Des. XXXX, XXX, XXX−XXX

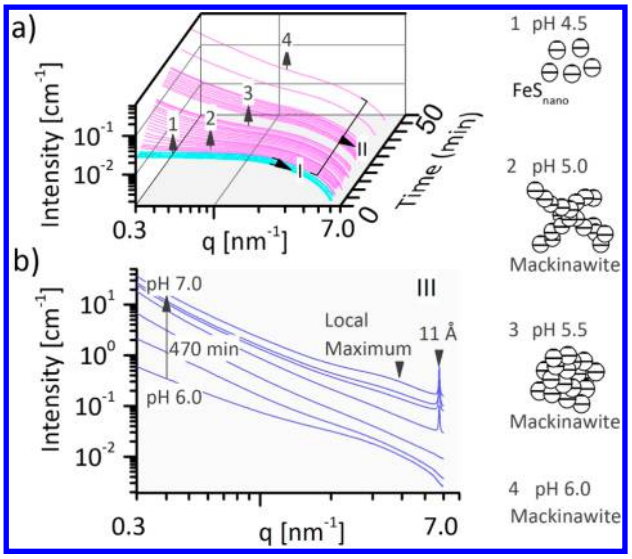

Figure 2. (a) In situ time-resolved SAXS patterns as a function of time from a titration experiment with 0.15 M NaHS, where we followed the formation and growth of mackinawite between pH 4.1 and 6.0 over the first 50 min of reaction (stages I–II, from Figure 1). As the reaction progressed in the first 50 min from pH 4.5 to 6.0, various solids were independently identified (numbers 1–4); (b) between pH 6.0 and 7.0 over the remaining 470 min (stage III, from Figure 1) of reaction showing the local maximum and the peak at 11 Å.

and the internal pores. In addition, a diffraction peak with a *d*-spacing of 11 Å (q of 5.72 nm^{-1}) appeared at pH 6.4 (Figure 2b and 2c).

We interpreted the changes in intensity in the first 50 min of the reaction in terms of aggregation of primary particles, in which very large aggregates are composed of a small population of primary particles, surrounded by the "sea" of nonaggregated primary particles. We fitted the SAXS data using a model that considers primary particles with the form factor $P(q)$ grouped into two populations: (1) noninteracting "loose" species and (2) species forming mass-fractal aggregates described by the structure factor $S(q)$. The model (eq 1) is expressed as a function of time, t, and we fitted the data between pH 4.1 and 6.4. This range of pH was chosen so as to include only frames collected before the development of the correlation maxima, and the appearance of the diffraction peak at 11 Å.

$$I(q, r_g, D, t) = N(\Delta\rho)^2 V^2 P(q, r_g)\left[\varepsilon(t) + (1 - \varepsilon(t))\left[1 + \frac{D\Gamma(D-1)\sin\left(\left(D-1\right)\frac{\pi}{2}\right)}{\left(\frac{r_g}{\sqrt{3/5}}q\right)^D}\right]\right] \quad (1)$$

In eq 1, N is a number density of primary particles, V is their volume and $\Delta\rho$ is a scattering contrast between the particles and the aqueous solvent. The prefactor $N(\Delta\rho)^2V^2$ is $I(q = 0)$ for the noninteracting particles. $P(q, r_g)$ is an approximation of the sphere form factor derived through the Guinier approximation, where the radius of a sphere $r_0 = (3/5)^{-1/2}r_g$; $\varepsilon(t)$ is a weight factor accounting for the relative contribution to scattering by loose particles; and $1 - \varepsilon(t)$ of those entangled in the mass-fractal-like aggregates, with values between 0 and 1.[7,24] The mass-fractal expression within the square brackets is a modified mass-fractal structure factor after Texeira et al. (1998),[25] with the original Teixera equation including the cutoff length, ξ, determining the size of the aggregates. However, since as described above we know that in our measurements the aggregates are infinite in size, we have simplified the equation with $\xi \to \infty$. Finally, D is the mass fractal dimension that relates the mass of the aggregates with the radius of gyration, Γ is the gamma function, and r_g is the radius of gyration of the primary particles (the same as in the form factor).

The first scattering patterns between pH 4.1 and 4.5 (<2.5 min, titration) were successfully fitted using only the sphere form factor expression. This indicated the formation of individual nanoparticles that are not spatially correlated with each other but that remained isolated from each other across this pH range. We documented in our previous work that, over this pH regime, a new nanoparticulate iron sulfide phase that we called FeS$_{nano}$ formed.[6] This phase, FeS$_{nano}$, has a distinct structure from mackinawite, and we showed that FeS$_{nano}$ is a crucial precursor for the formation of mackinawite.[6] In the experiments discussed here, we confirmed that these primary nanoparticles were spherical in shape and that their radius of gyration (r_g) remained constant (0.46 ± 0.01 nm) not just between pH 4.1 and 4.5, but all the way to pH 5.9, which is actually outside the stability field of FeS$_{nano}$[6] (Figure 3). These

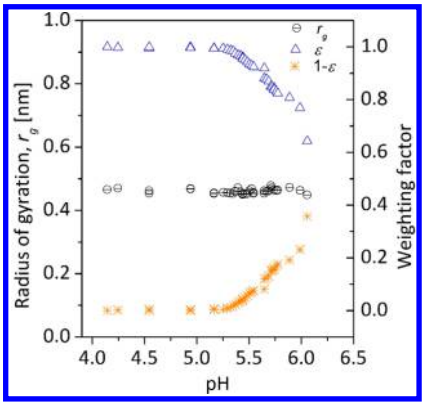

Figure 3. Parameters derived from fitting from mass fractal structure factor: (a) radius of gyration, r_g; (b) weighting factor *eta*.

initial isolated small particles rapidly aggregated to form mass fractal-like structures with a constant mass fractal dimension (D) of 1.94, just above pH ~4.5. The fractal-like structures constantly grew up to pH ~6, when their contribution to scattering expressed as $1 - \varepsilon_{(t)}$ reached ~40% (Figure. 3). As the pH increased further, the intensity continuously increased and the linear region extended to high-q. The previously observed features related to the form factor disappeared as the reaction progressed toward pH 7.0, suggesting the coalescence of the already formed aggregates (Figure. 2b).

The scattering model used to describe the SAXS data suggests that other types of aggregates also exist (Figure 2); these aggregates consist of internally correlated structures with r_0 < 0.50 nm, and they revealed *d*-spacings of ~0.9 nm based on the hard sphere structure factor models. The simultaneous appearance of these small clusters with the above-described

DOI: 10.1021/acs.cgd.8b01025
Cryst. Growth Des. XXXX, XXX, XXX–XXX

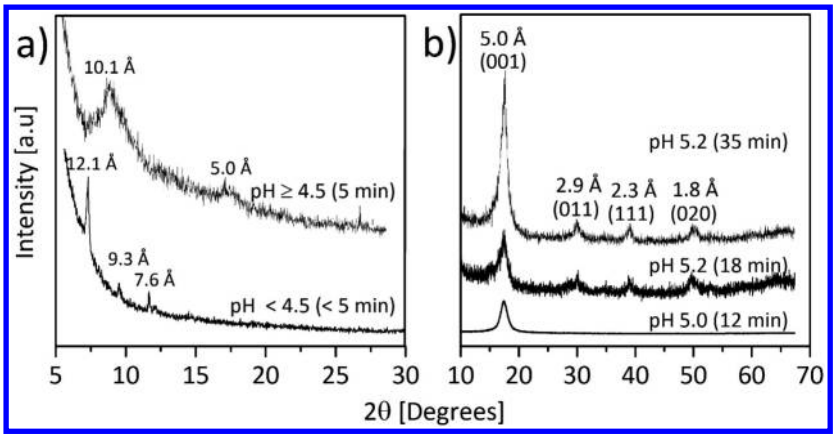

Figure 4. XRD patterns of (a) FeS_{nano} formed below pH 4.5 showing three low angle diffraction peaks above 7 Å (bottom), and a diffraction pattern (top) showing an expanded diffraction peak at ∼10 Å from FeS_{nano} and at ∼5.0 Å peak from mackinawite as the pH was raised above 4.5; (b) poorly crystalline mackinawite developing further above pH 5.0.

bigger aggregates imply that these clusters consisted of few primary particles that could have been either detached from the bigger aggregates as small aggregates or clusters of few primary particles that could themselves have detached from the bigger aggregates and subsequently aggregated.

From fitting the SAXS data for the whole process we can conclude that the formation of mackinawite was preceded by the nucleation and growth of primary FeS_{nano} particles (<pH = 4.5) that subsequently aggregated to form mass fractal-like structures that continuously grew until pH ∼6.0, and then coalesced to form larger aggregates. Based on off-line solid characterization with XRD, we also show that the FeS_{nano} phase that was stable only at a pH below 4.5 and it was characterized by three diffraction peaks with *d*-spacings of 12.1, 9.3, and 7.6 Å (Figure 4a). Once the pH was raised to ≥4.5 and the FeS_{nano} started aggregating and coalescing, we observed the transition from FeS_{nano} to mackinawite, as evidenced in Figure 4a (upper pattern). The appearance of a diffraction peak with *d*-spacings of 10.1 Å indicates the expanded planes of the FeS_{nano}, and the Bragg peak at 5.0 Å indicates the emerging poorly ordered (001) plane of mackinawite. With time and at even higher pH (above 5.0), the evolution towards mackinawite was confirmed through the coappearance of the other characteristic diffraction peaks for mackinawite (i.e., 011, 111, 020) (Figure. 4b).

We confirmed the transformation from FeS_{nano} to mackinawite also through HR-TEM images and analyses. Images of solids collected below pH 4.5 revealed that primary FeS_{nano} particles ∼2 nm in size[6] that randomly orient themselves into clusters that can reach ∼20−30 nm in diameter (Figure 5a). Fast Fourier transform (FFT) analyses of such clusters showed not only the large *d*-spacings characteristic for FeS_{nano} (∼10 and ∼7 Å) but also *d*-spacings closer to those characteristic for a mackinawite-like structure (Figure 5a, *d*-spacing ∼5.5 Å). With time the cluster aggregated into large, hundreds of nanometers structures (Figure 5b). Selected area electron diffraction (SAED) patterns of these emerging branched aggregate networks showed diffuse rings with *d*-spacings of 3.2, 1.9, and 1.4 Å that correspond to mackinawite (Figure 5b). With continuing reaction progress (increase in pH and time), the poorly ordered nature of the mackinawite in the aggregates increased and the structures became denser, larger, and more crystalline. This is reflected in a diffraction pattern consisting mainly of discrete diffraction bands with spots from single

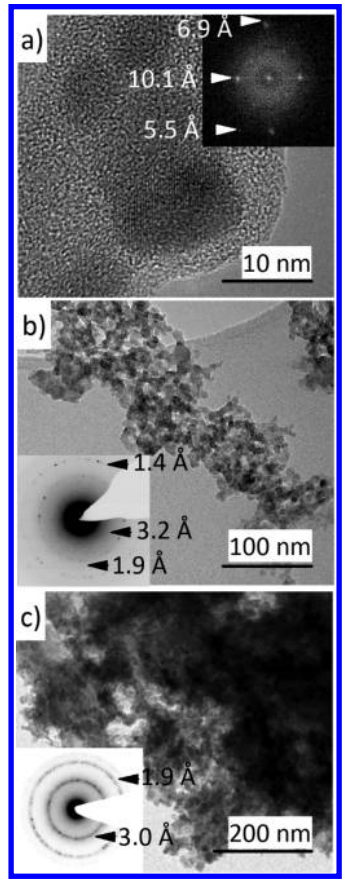

Figure 5. (a) HR-TEM image from clusters with individual primary FeS_{nano} particles; inset is an FFT showing crystalline fringes with *d*-spacings for both FeS_{nano} and a mackinawite-like phase; (b) fractal aggregates in a branched network formed at pH above ∼4.5 with inset showing the SAED pattern; (c) large and dense aggregates formed at pH 4.6, with inset showing their SAED pattern.

crystal-like arrangements within the aggregates and the evolution of a polycrystalline phase (insets in Figure 5b and 5c).

When such aggregates were formed in the diffusion experiments and left reacting at pH 4.5 for 24 h, they also formed mass fractal-like aggregates, but in this case, these adopted rounded and more compact morphologies (Figure 6a)

DOI: 10.1021/acs.cgd.8b01025
Cryst. Growth Des. XXXX, XXX, XXX−XXX

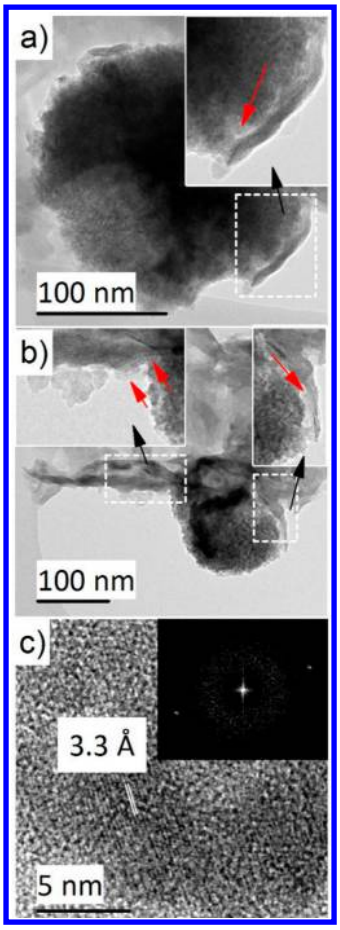

Figure 6. Bright field TEM images showing (a) rounded aggregates ~200 nm in diameter composed of FeS_{nano} primary particles; (b) transformation of rounded aggregates to form layered mackinawite; the arrows in (a) and (b) indicate the location where the Fe−S particles initiated the self-assembling to form layered mackinawite; (c) HR-TEM image of Fe−S primary particles showing oriented aggregation to form the initial mass-fractal clusters; the corresponding FFT of the image confirms the crystallographic orientation.

or a layered structure in which particles crystallographically aligned themselves through an oriented aggregation (OA) mechanism (Figure 6b and 6c). This alignment was not always perfect, as stacking faults were observed along the 001 plane (Figure 7a). Nevertheless, the resulting phase showed a two-dimensional morphology composed of ~3−8 ordered atomic layers separated by ~6.8 Å (Figure 7a and 7b), a *d*-spacing which was previously reported for disordered machinawite.[2] The SAED pattern of such layered structures revealed a combination of diffuse rings and bright spots with *d*-spacings of 4.9 Å (001 plane, nominally 5.03 Å), 2.9 Å (011 plane, nominally 2.97 Å), and 2.1 Å that relate to the mackinawite structure (Figure 7b).

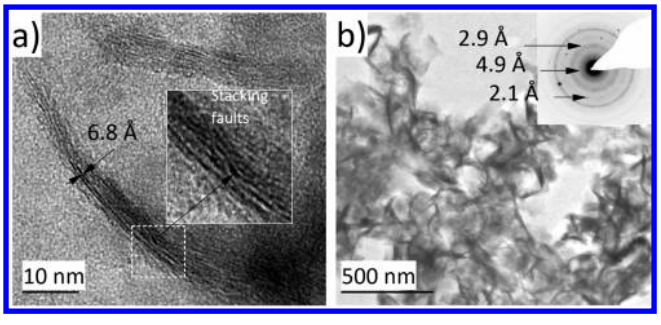

Figure 7. (a) Detail of the atomic layers of poorly ordered mackinawite still showing 6.8 Å distances with visible stacking faults. (b) Moderately ordered Mackinawite arranged in a 2D layered morphology with the corresponding SAED pattern showing the almost typical *d*-spacings of mackinawite.

When a limited input of H_2S was maintained (as in the 1 h diffusion experiment), mackinawite aggregates formed soon after the appearance of FeS_{nano} (Figure 8a). Likewise, with a limited but prolonged H_2S addition (as in the 24 h diffusion experiment), the process proceeded in the same manner but the formed aggregates rearranged into rounded, bigger, and denser structures that later formed layered mackinawite (Figure 8b). On the other hand, when H_2S addition was continuous (titration), and the pH increased above 4.5, aggregates and mass fractal structures grew in number but not significantly in size (up to 10−14 nm) (Figure 8c). When the pH subsequently increased rapidly from 4 to 7, very large aggregates formed possibly under an OA or cluster-to-cluster aggregation mechanism (Figure 8d).

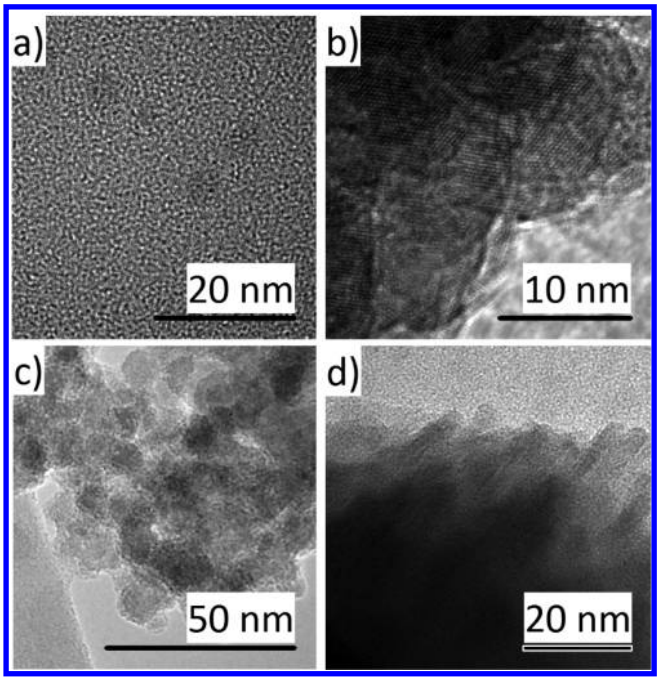

Figure 8. Images comparing the aggregates from (a) 1 h of diffusion; (b) 24 h of diffusion; (c) slow titration, solid separated at pH 4.5; and (d) fast titration, solid separated at pH 7.

In our experiments, mackinawite formation starts with the homogeneous nucleation of the FeS_{nano} precursor just slightly above pH ~4.1 (pH of the starting Fe^{2+} solution) induced by the initial diffusion of H_2S_{gas} or the titration with NaHS. In a second stage these FeS_{nano} primary particles aggregate into branched networks. The aggregation process itself was observed in both titration and diffusion experiments regardless of how precipitation was induced (Figures 5b and 6a). These initial aggregates gradually become more stable by first forming rounded morphologies and then more stable layered structures; however, this process depends on the constant addition of H_2S (gradual pH increase), as otherwise the formed FeS_{nano} phases could partially dissolve. This is

DOI: 10.1021/acs.cgd.8b01025
Cryst. Growth Des. XXXX, XXX, XXX−XXX

explained when one assumes equilibrium between Fe^{2+} and H_2S ($FeS + 2H^+ = [Fe^{2+}] + H_2S^0$; $pk = 4.5$ at 25 °C,[26,27] and one calculates the equilibrium ion concentrations for $[Fe^{2+}]$ and $[H_2S]$ to be ~0.018 M at pH 4.1. Since the initial $[Fe^{2+}]$ concentration was 0.1 M, immediately upon the first addition of sulfide and the first precipitation at pH 4.1, ~18% of the formed primary FeS_{nano} phase would immediately redissolve. However, as the pH increases to ~4.5, the dissolved $[Fe^{2+}]$ remaining in solution is 0.0058 M and only ~6% of the primary FeS_{nano} phase would redissolve. Considering that the poorly ordered and layered mackinawite started to form only at a pH above 4.5 after the primary particles aggregated, these initial nanophases still remain present in the mix (as shown by SAXS), as they would become less susceptible of dissolution. This also explains why the initial mackinawite structure is poorly ordered with larger *d*-spacings and only with increasing pH and time does it arrange itself into a more stable structural configuration.

Based on our results, we can infer that the formation of mackinawite follows a nonclassical nucleation and growth pathway via oriented aggregation (OA). Our observations point to a five-stage process (Figure 9) in accordance with the

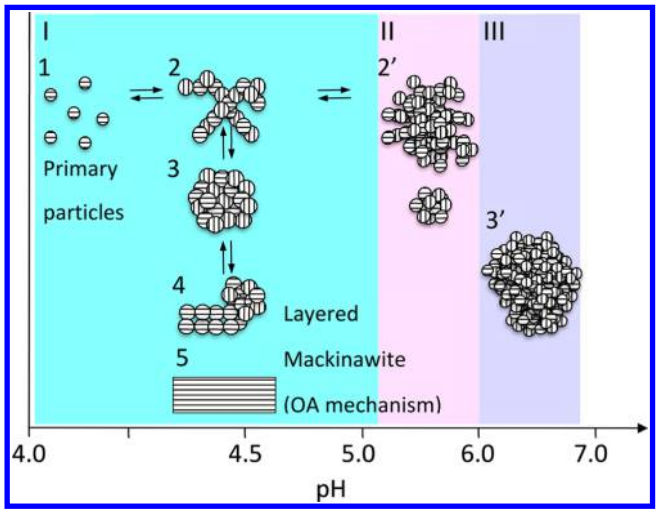

Figure 9. Nonclassical growth of mackinawite following an oriented aggregation mechanism. Morphology changes incurred in stage I between pH 4.1 and 5.2: (1) Primary particles, (2) reversible aggregation into a mass fractal structures with internal correlations; (3, 4) self-assembly of particles into an aligned crystallographic arrangement; (5) formation of layered mackinawite structure. The continuous formation of aggregates (2′) follows in stage II between pH 5.2 and 6.0; upon continuous addition of H_2S (pH increase) the aggregates reach bigger and denser morphologies (3′) up to pH 7.0.

OA process proposed:[11,28−30] homogeneous nucleation of primary FeS_{nano} particles (1), formation of reversible mass fractal-like (2, 3) or cluster-to-cluster aggregates from the FeS_{nano} (2′−3′); oriented alignment and self-assembly of mackinawite-like particles (4), and formation of a typical metastable layered mackinawite structure (5).

Self-assembly of particles through OA has been reported for many other mineral systems (e.g., magnetite, goethite, apatite, ferrihydrite),[28,31−35] and the crystallization of these minerals through particle aggregation was reported to include stages of multiple ion complexes and all the way to transformations to fully formed nanocrystals.[36] Our results demonstrate that, in the iron−sulfide system, an initial nanocrystalline FeS_{nano} transforms into more stable and poorly crystalline mackinawite via aggregation or self-assembly of the structure. Such self-assembly reactions leading to the formation of a stable ZnS and CdS nanoparticle were described before,[37] yet so far this has not been documented in the Fe−S system. This is likely because the reactions are extremely rapid and the intermediates are highly unstable. However, similarly to other systems in our work we showed that, in the OA process, particles aligned parallel to crystallographic planes to form bigger agglomerated structures (Figure 6a). The so formed initial poorly ordered mackinawite-like phase gradually evolves toward a more ordered and nanocrystalline state with its structure progressing from expanded *d*-spacings between the Fe−S tetrahedral layers (i.e., 6.8 Å), toward the typical distance of 5.0 Å in more-crystalline mackinawite. The initial expanded layered structure could accommodate the incorporation of trace metals or organic molecules in between the layers, making this structure very attractive for the potential incorporation of harmful elements for remediation purposes.

Our results suggest that pH and the rates of reaction between iron and sulfide are the main factors affecting the morphology of any resulting mackinawite (Figure 8).

CONCLUSION

After rapid nucleation, through a nanoparticulate precursor, mackinawite growth follows an oriented aggregation pathway that involves arrangement and self-assembly. This leads to different morphologies that are highly dependent on pH and the rates of reaction. Aggregation into mass fractal-like structures made up of primary particles is an important step in mackinawite formation, and the subsequent self-assembly of these aggregates to reach stable structures leads to the final metastable nanocrystalline mackinawite phase. With this work, we documented the mechanistic aspects for the formation and growth of mackinawite. Mackinawite is an important intermediate phase that is relevant in numerous geochemical processes in modern and ancient environments, but the findings described above can be also important for the development of novel, highly reactive, yet controllable nanomaterials for industrial applications (e.g., catalysis, CO_2 reduction, electronics, energy storage, and remediation). For example, mackinawite formed at low pH can be highly reactive due to the small size of its constituent particles and the fact that it forms highly disordered mass fractals that are very reactive and therefore useful for applications in remediation and in the synthesis of green catalysts. Mackinawite with an expanded layered structure has advantages for remediation purposes, but also this morphology is very attractive in the development of materials for energy conversion and storage and in the development of superconductors.

AUTHOR INFORMATION

Corresponding Authors

*E-mail: A.MatamorosVeloza@leeds.ac.uk (A.M.V.).
*E-mail: benning@gfz-potsdam.de (L.G.B).

ORCID

Adriana Matamoros-Veloza: 0000-0002-3870-9141

Notes

The authors declare no competing financial interest.

DOI: 10.1021/acs.cgd.8b01025
Cryst. Growth Des. XXXX, XXX, XXX−XXX

■ ACKNOWLEDGMENTS

We would like to acknowledge the Natural Environment Research Council (Grant NE/J008745/1) for financial support for this work. We acknowledge Diamond Light Source Ltd. (UK) for beamtime allocation at I22 (SM8973) and the help of N. Terril and A. Smith. Also, we thank M. Ward and the Leeds Electron Microscopy and Spectroscopy Centre for help with TEM imaging and analyses. This research was partially made possible by a Marie Curie grant from the European Commission: the NanoSiAl Individual Fellowship, Project No. 703015. We also acknowledge the financial support of the Helmholtz Recruiting Initiative grant No. I-044-16-01.

■ REFERENCES

(1) Rickard, D.; Luther, G. W. Chemistry of Iron Sulfides. *Chem. Rev.* **2007**, *107*, 514−562.
(2) Csákberényi-Malasics, D.; Rodriguez-Blanco, J. D.; Kis, V. K.; Rečnik, A.; Benning, L. G.; Pósfai, M. Structural properties and transformations of precipitated FeS. *Chem. Geol.* **2012**, *294-295*, 249−258.
(3) Wächtershäuser, G. Life as We Don't Know It. *Science* **2000**, *289*, 1307−1308.
(4) Benning, L. G.; Wilkin, R. T.; Barnes, H. L. Reaction pathways in the Fe−S system below 100°C. *Chem. Geol.* **2000**, *167*, 25−51.
(5) Hunger, S.; Benning, L. G. Greigite: a true intermediate on the polysulfide pathway to pyrite. *Geochem. Trans.* **2007**, *8*, 1−20.
(6) Matamoros-Veloza, A.; Cespedes, O.; Johnson, B. R. G.; Stawski, T. M.; Terranova, U.; de Leeuw, N. H.; Benning, L. G. A highly reactive precursor in the iron sulfide system. *Nat. Commun.* **2018**, *9*, 3125.
(7) Weatherill, J. S.; Morris, K.; Bots, P.; Stawski, T. M.; Janssen, A.; Abrahamsen, L.; Blackham, R.; Shaw, S. Ferrihydrite Formation: The Role of Fe13 Keggin Clusters. *Environ. Sci. Technol.* **2016**, *50*, 9333−9342.
(8) Rodriguez-Blanco, J. D.; Shaw, S.; Benning, L. G. The kinetics and mechanisms of amorphous calcium carbonate (ACC) crystallization to calcite, via vaterite. *Nanoscale* **2011**, *3*, 265−271.
(9) Stawski, T. M.; van Driessche, A. E. S.; Ossorio, M.; Diego Rodriguez-Blanco, J.; Besselink, R.; Benning, L. G. Formation of calcium sulfate through the aggregation of sub-3 nanometre primary species. *Nat. Commun.* **2016**, *7*, 11177.
(10) Benning, G. L.; Waychunas, A. G. Nucleation, Growth, and Aggregation of Mineral Phases: Mechanisms and Kinetic Controls. In *Kinetics of Water-Rock Interaction*; Brantley, L. S., Kubicki, D. J., White, F. A., Eds.; Springer New York: New York, NY, 2008; pp 259−333, DOI: 10.1007/978-0-387-73563-4_7.
(11) Penn, R. L.; Banfield, J. F. Oriented attachment and growth, twinning, polytypism, and formation of metastable phases; insights from nanocrystalline TiO2. *Am. Mineral.* **1998**, *83*, 1077−1082.
(12) Bots, P.; Benning, L. G.; Rodriguez-Blanco, J.-D.; Roncal-Herrero, T.; Shaw, S. Mechanistic Insights into the Crystallization of Amorphous Calcium Carbonate (ACC). *Cryst. Growth Des.* **2012**, *12*, 3806−3814.
(13) Van Driessche, A. E. S.; Benning, L. G.; Rodriguez-Blanco, J. D.; Ossorio, M.; Bots, P.; García-Ruiz, J. M. The Role and Implications of Bassanite as a Stable Precursor Phase to Gypsum Precipitation. *Science* **2012**, *336*, 69−72.
(14) Bergström, L.; Sturm, E. V.; Salazar-Alvarez, G.; Cölfen, H. Mesocrystals in Biominerals and Colloidal Arrays. *Acc. Chem. Res.* **2015**, *48*, 1391−1402.
(15) Sturm, E. V.; Cölfen, H. Mesocrystals: structural and morphogenetic aspects. *Chem. Soc. Rev.* **2016**, *45*, 5821−5833.
(16) Yang, Y.; Wang, Q.; Liu, Z.; Jin, L.; Ou, B.; Han, P.; Wang, Q.; Cheng, X.; Liu, W.; Wen, Y.; Liu, Y.; Zhao, W. Self-Assembly of ZnO Nanoplatelets into Hierarchical Mesocrystals and Their Photocatalytic Property. *IOP Conf. Ser.: Mater. Sci. Eng.* **2018**, *317*, 012076.
(17) Wu, H.; Yang, Y.; Ou, Y.; Lu, B.; Li, J.; Yuan, W.; Wang, Y.; Zhang, Z. Early Stage Growth of Rutile Titania Mesocrystals. *Cryst. Growth Des.* **2018**, *18*, 4209−4214.
(18) Yuwono, V. M.; Burrows, N. D.; Soltis, J. A.; Penn, R. L. Oriented Aggregation: Formation and Transformation of Mesocrystal Intermediates Revealed. *J. Am. Chem. Soc.* **2010**, *132*, 2163−2165.
(19) Rao, A.; Drechsler, M.; Schiller, S.; Scheffner, M.; Gebauer, D.; Cölfen, H. Stabilization of Mineral Precursors by Intrinsically Disordered Proteins. *Adv. Funct. Mater.* **2018**, *28*, 1802063.
(20) Cahill, C. L.; Benning, L. G.; Barnes, H. L.; Parise, J. B. In situ time-resolved X-ray diffraction of iron sulfides during hydrothermal pyrite growth. *Chem. Geol.* **2000**, *167*, 53−63.
(21) Zhang, F.; Ilavsky, J.; Long, G. G.; Quintana, J. P. G.; Allen, A. J.; Jemian, P. R. Glassy Carbon as an Absolute Intensity Calibration Standard for Small-Angle Scattering. *Metall. Mater. Trans. A* **2010**, *41*, 1151−1158.
(22) Basham, M.; Filik, J.; Wharmby, M. T.; Chang, P. C. Y.; El Kassaby, B.; Gerring, M.; Aishima, J.; Levik, K.; Pulford, B. C. A.; Sikharulidze, I.; Sneddon, D.; Webber, M.; Dhesi, S. S.; Maccherozzi, F.; Svensson, O.; Brockhauser, S.; Náray, G.; Ashton, A. W. Data Analysis WorkbeNch (DAWN). *J. Synchrotron Radiat.* **2015**, *22*, 853−858.
(23) Lennie, A.; Redfern, S. A.; Schofield, P.; Vaughan, D. Synthesis and Rietveld crystal structure refinement of mackinawite, tetragonal FeS. *Mineral. Mag.* **1995**, *59*, 677−683.
(24) Stawski, T. M.; Veldhuis, S. A.; Besselink, R.; Castricum, H. L.; Portale, G.; Blank, D. H. A.; ten Elshof, J. E. Nanoscale Structure Evolution in Alkoxide−Carboxylate Sol−Gel Precursor Solutions of Barium Titanate. *J. Phys. Chem. C* **2011**, *115*, 20449−20459.
(25) Texeira, J. Small-angle scattering by fractal systems. *J. Appl. Crystallogr.* **1998**, *21*, 781−875.
(26) Davison, W.; Phillips, N.; Tabner, J. B. Soluble iron sulfide species in natural waters: Reappraisal of their stoichiometry and stability constants. *Aquat. Sci.* **1999**, *61*, 23−43.
(27) Bourdoiseau, J.-A.; Jeannin, M.; Rémazeilles, C.; Sabot, R.; Refait, P. The transformation of mackinawite into greigite studied by Raman spectroscopy. *J. Raman Spectrosc.* **2011**, *42*, 496−504.
(28) Penn, R. L. Kinetics of oriented aggregation. *J. Phys. Chem. B* **2004**, *108*, 12707−12712.
(29) Soltis, J. A.; Penn, R. L. Oriented Attachment and Nonclassical Formation in Iron Oxides. In *Iron Oxides*; Wiley-VCH Verlag GmbH & Co. KGaA: 2016; pp 243−268, DOI: 10.1002/9783527691392.ch11.
(30) Burrows, N. D.; Hale, C. R. H.; Penn, R. L. Effect of pH on the Kinetics of Crystal Growth by Oriented Aggregation. *Cryst. Growth Des.* **2013**, *13*, 3396−3403.
(31) Wan, J.; Tang, J.; Zhang, C.; Yuan, R.; Chen, K. Insight into the formation of magnetite mesocrystals from ferrous precursors in ethylene glycol. *Chem. Commun.* **2015**, *51*, 15910−15913.
(32) Yan, W.; Liu, H.; Chen, R.; Xie, J.; Wei, Y. Dissolution and oriented aggregation: transformation from lepidorocite to goethite by the catalysis of aqueous Fe(II). *RSC Adv.* **2015**, *5*, 106396−106399.
(33) Iafisco, M.; Ramirez-Rodriguez, G. B.; Sakhno, Y.; Tampieri, A.; Martra, G.; Gomez-Morales, J.; Delgado-Lopez, J. M. The growth mechanism of apatite nanocrystals assisted by citrate: relevance to bone biomineralization. *CrystEngComm* **2015**, *17*, 507−511.
(34) Penn, R. L.; Soltis, J. A. Characterizing crystal growth by oriented aggregation. *CrystEngComm* **2014**, *16*, 1409−1418.
(35) Li, D.; Nielsen, M. H.; Lee, J. R. I.; Frandsen, C.; Banfield, J. F.; De Yoreo, J. J. Direction-Specific Interactions Control Crystal Growth by Oriented Attachment. *Science* **2012**, *336*, 1014−1018.
(36) De Yoreo, J. J.; Gilbert, P. U. P. A.; Sommerdijk, N. A. J. M.; Penn, R. L.; Whitelam, S.; Joester, D.; Zhang, H.; Rimer, J. D.; Navrotsky, A.; Banfield, J. F.; Wallace, A. F.; Michel, F. M.; Meldrum, F. C.; Cölfen, H.; Dove, P. M. Crystallization by particle attachment in synthetic, biogenic, and geologic environments. *Science* **2015**, *349*, aaa6760.

DOI: 10.1021/acs.cgd.8b01025
Cryst. Growth Des. XXXX, XXX, XXX−XXX

(37) Huang, F.; Gilbert, B.; Zhang, H.; Banfield, J. F. Reversible, Surface-Controlled Structure Transformation in Nanoparticles Induced by an Aggregation State. *Phys. Rev. Lett.* **2004**, *92*, 155501.

DOI: 10.1021/acs.cgd.8b01025
Cryst. Growth Des. XXXX, XXX, XXX−XXX